Polymer 54 (2013) 6654–6662

Contents lists available at ScienceDirect

Polymer

journal homepage: www.elsevier.com/locate/polymer

Crystallization and microstructure of poly(butylene oxalate)

Pei-Chun Kuo, Chieh-Tsung Lo*, Chuh-Yung Chen

Department of Chemical Engineering, National Cheng Kung University, No. 1, University Road, Tainan City 701, Taiwan

ARTICLE INFO

Article history:
Received 10 May 2013
Received in revised form
23 August 2013
Accepted 6 October 2013
Available online 11 October 2013

Keywords:
Poly(butylene oxalate)
Isothermal crystallization
Lamellar thickness

ABSTRACT

Crystal structure and morphology development of poly(butylene oxalate) (PBOX) during isothermal crystallization were studied with X-ray diffraction, time-resolved simultaneous small-angle X-ray scattering, differential scanning calorimetry, and optical microscopy. Results indicate that the decrease in the long period at low crystallization temperature indicated the occurrence of secondary crystallization in the interlamellar space. Meanwhile, the lamellar thickness slightly increased with crystallization temperatures due to the formation of thicker crystalline layers at high temperatures. The crystal growth rate of PBOX was analyzed by optical microscopy. Using values of the equilibrium melting temperature of 117.4 °C and the fold surface free energy of 32.37 erg/cm^2 obtained by the Gibbs–Thomson theory, the nucleation parameter, K_g, of 97264 K^2 and the lateral surface free energy of 17.68 erg/cm^2 were determined from the Lauritzen and Hoffman equation. These values are comparable to various semicrystalline polymers previous reported and are not available up to now for PBOX in the literature.

© 2013 Elsevier Ltd. All rights reserved.

1. Introduction

There has been a growing interest in developing biodegradable polymers for a wide variety of applications, including packaging, tissue engineering, and drug delivery. Biodegradable polymers are obtainable from environmentally friendly materials, such as agriculture crops. This makes biodegradable polymers are recyclable and bio-resolvable and they can be obtained in abundance and low cost. Thus, the use of them has significance in the sustainable development and environment protection. On the other hand, most of the conventional non-degradable thermoplastics are originated from the petroleum resource that may cause the depletion of the resource. Although the development of biodegradable polymers is undoubted the immanent task to achieve, the use of agricultural resources to produce biodegradable polymers may also generate numerous issues, such as the limited availability of foodstuff and the competition between food and non-food production in critical geographic areas. Polyoxalates, which are produced mostly from grass, seem more suitable to be used in the biocompatible materials.

A polyoxalate has an ester backbone, which can be hydrolytically cleaved to produce propylene glycol and oxalic acid. Since the pioneering work on polyoxalates investigated by Carothers et al. [1], both the synthesis and applications of polyoxalates are the subject of research by many groups. The polyoxalates are synthesized from a two-step reaction. The first step lies in the ester interchange reaction of diols with ester of oxalic acid to form a prepolymer [2]. Further postpolymerization under heat and reduced pressure completes the second step to obtain the polymer. The synthesized polyoxalates are characterized to be hydrophobic and have satisfactory mechanical properties. This makes polyoxalates highly appropriate for practical use, including drug delivery [3,4] and the water treatment for the removal of heavy metal ions [5]. Ballistreri et al. [6] investigated the primary thermal decomposition of poly(ethylene oxalate) and found that the intramolecular exchange reactions predominated in the primary thermal fragmentation processes, resulting in the formation of cyclic oligomers up to tetramer. Thibeault et al. [7] further proposed the competing mechanism of thermal decomposition of polyoxalates through depolymerization, fragmentation to polyenes and CO_2, and crosslinking. When poly(ethylene oxalate) was heated to 170–260 °C, polycondensation, depolymerization, and decomposition occurred and the process of decomposition was second order [8]. Finelli et al. investigated the thermal properties of poly(butylene oxalate) and its random copolymer with azelaic acid [9]. The content of the azelaic acid in copolymer mainly caused decreases in both the melting and glass transition temperatures. In addition to the thermal properties and thermal decomposition of polyoxalates, one of the most dominant factors to develop polyoxalates is the crystallization behavior. In the application point of view, specific crystal morphology determines the final properties of the

* Corresponding author. Tel.: +886 6 2757575x62647; fax: +886 6 2344496.
E-mail addresses: chiehtsung06@yahoo.com.tw, tsunglo@mail.ncku.edu.tw (C.-T. Lo).

0032-3861/$ – see front matter © 2013 Elsevier Ltd. All rights reserved.
http://dx.doi.org/10.1016/j.polymer.2013.10.015

materials. For instance, when drug delivery is considered, crystalline regions do not erode at the same rate as amorphous regions [10]. The hydrolysis of the crystalline polymers is prolonged when compared to their amorphous counterparts [11]. The crystal morphology of polymers also plays a key role on the adhesion formation after peritoneal surgery [11]. Up to date, however, studies on the polyoxalate crystallization are limited.

In this work, we investigate the isothermal crystallization of a member of polyoxalate family, namely poly(butylene oxalate) (PBOX), using X-ray diffraction, *in situ* small angle X-ray scattering, differential scanning calorimetry, and optical microscopy. The structural parameters, including the long period, lamellar thickness, and degree of crystallinity, were obtained to form a comprehensive picture of the crystal morphology. The combination of these techniques provides information not only on the lamellar dimensions but also the crystallization mechanism of PBOX. The knowledge of the microstructure of the PBOX, coupled with its crystallization behavior and thermal properties, will help to guide the rational design of polyoxalates for various applications.

2. Experimental section

2.1. Materials

PBOX was synthesized, according to a literature method, by a two step reaction [6,8]. Briefly, 1 mol diethyl oxalate (Acros Organics) and 1.2 mol 1,4-butanediol (Alfa Aesar) were mixed in a reactor. Tetrabutyl titanate ($Ti(OBu)_4$, Sigma–Aldrich) was used as a catalyst and the mixture was kept at 140–160 °C for 4 h. After solidification and removal of alcohol, the transesterification was carried out at 180 °C for 4 h under a pressure of 1–3 torr to synthesize PBOX. The prepared PBOX has the molecular weight of about 10,000 g/mol and the glass transition temperature of −20 °C.

2.2. X-ray diffraction (XRD)

X-ray diffraction analysis of the examined materials was performed at room temperature using a Rigaku RINT-2000 diffractometer coupled to a source of filtered CuK_α radiation. Data were collected in the angle scan from 10° to 80° with a scan rate of 5°/min.

2.3. Small angle X-ray scattering (SAXS)

Samples for SAXS measurement were prepared via the melting of PBOX into DSC aluminum sample pans (Perkin Elmer). The sample thickness was 1 mm. The sample pans made ideal sample holders because the aluminum was fairly transparent to the high-brilliance X-rays, and the rigid pans maintained the sample thickness when the polymer was melted in the vertically mounted SAXS sample chamber [10]. The SAXS measurements were conducted in Sector 23A1 at the National Synchrotron Radiation Research Center in Taiwan. The incident beam energy was 8 keV. A two-dimensional CCD detector, at a distance of 2 m from the sample, was used to measure the intensity of scattering. During SAXS measurement, the samples were initially equilibrated at 120 °C, which is above the melting temperature of PBOX, for at least 20 min. Samples were rapidly quenched to a crystallization temperature to allow for crystallization. Data were collected at 10-sec intervals during isothermal crystallization over the range of the scattering vector (q) from 0.006 to 0.27 $Å^{-1}$, where $q = 4\pi\sin(\theta/2)/\lambda$, θ is the scattering angle, and λ is the incident radiation wavelength. The scattering data were appropriately corrected for incident flux, absorption, detector sensitivity variation, and dark current, and the scattering intensity was azimuthally averaged to obtain the one-dimensional intensity data [$I(q)$] as a function of q.

2.4. Differential scanning calorimetry (DSC)

The thermal properties of PBOX were measured using a scanning differential calorimeter (DSC 7, Perkin Elmer). Samples of ~5 mg were heated from 25 °C to 120 °C with a heating rate of 10 °C/min and the melting temperature of PBOX crystallized at different temperatures was analyzed. Melting temperatures were calibrated with indium and tin standards and were reported as the peak in the melting endotherm.

2.5. Optical microscopy

Optical microscopy was carried out with a Nikon H550L Eclipse 50i LV-UEPI microscope in conjunction with a hot stage. Samples were prepared by dropping polymer solution on a glass slide to form a specimen with a thickness of ~20 μm. The specimen was heated to 120 °C for 20 min to remove the residual crystals and was rapidly quenched to the desired crystallization temperatures to allow for PBOX crystallization. The growth of spherulites was recorded using a Sony color video camera (SSC-DC80 Super Exwave) and the radii of the spherulites as a function of time were measured from time-lapsed frames of spherulitic front. Reported spherulitic growth rates (G) were determined as the mean of the rates from at least 20 spherulites, monitored on from several samples.

2.6. SAXS analysis

Before the extraction of the morphological parameters of interest from the SAXS measurements, the data have to be extrapolated to both the high and low q regions [12]. Extrapolation to q = zero in the region of the beam stop was accomplished by the extrapolation of the intensity using Debye–Bueche approximation [13]

$$I(q) = \frac{I(0)}{\left(1 + q^2\xi^2\right)^2} \tag{1}$$

where ξ is the correlation length. On the other hand, the extrapolation in the high q region was performed with the aid of the Porod law [14]

$$I(q) = \frac{K_p}{q^4}\exp\left(-\sigma_1^2 q^2\right) + I_b \tag{2}$$

here, I_b is the contribution to scattering from local electron density fluctuations in the amorphous phase, K_p is a Porod law constant, and σ_1 is the transition thickness between crystalline and amorphous phases.

The one-dimensional correlation function, $\gamma(r)$, which offers more details of the microstructure, is the Fourier transform of the corrected SAXS data, given by Ref. [15].

$$\gamma(r) = \frac{1}{Q}\int_0^\infty q^2 I(q)\cos(qr)dq \tag{3}$$

where Q is the invariant. The invariant is computed for each file as the area under the Lorentz-corrected intensity profile [15].

$$Q = \int_0^\infty q^2 I(q) dq = W_c(1 - W_c)(\eta_c - \eta_a)^2 \quad (4)$$

here, W_c and η_c are the linear degree of crystallinity and electron density in the crystalline phase and η_a is the electron density in the amorphous phase. From $\gamma(r)$, the average long period (L) can be determined from the first maximum of the correlation curve. By the assumption of the two-phase model proposed by Strobl and Schneider [15], the linear degree of crystallinity within the lamellar stacks can be estimated from the correlation function

$$\gamma_0/L = W_c(1 - W_c) \quad (5)$$

where γ_0 is the ordinate corresponding to the first zero of the abscissa in the correlation function. It has to be pointed out that Eq. (5) only stands for $W_c > 0.5$. When $W_c < 0.5$, W_c is replaced by $(1 - W_c)$ in the above expression. After the linear degree of crystallinity has been obtained, the average lamellar thickness (l_c) can be estimated as the product of the long period and the linear degree of crystallinity. The difference between the long period and the lamellar thickness gives the average amorphous layer thickness (l_a).

3. Results and discussion

3.1. Bulk crystallinity

Fig. 1 presents diffractograms of the PBOX crystallized at various crystallization temperatures for several days. The diffractograms obtained for the PBOX crystallized at these temperatures exhibited very similar diffraction peaks, suggesting the nearly identical crystallographic morphology of PBOX crystallized at these temperatures. Analyzed by indexing software Dicvol 91, the evolution of the triclinic crystal structure can be followed by the appearance of several reflections, which are marked in Fig. 1. The triclinic structure in PBOX has the unit cell dimensions of $a_0 = 0.852$ nm, $b_0 = 0.475$ nm, $c_0 = 0.761$ nm, $\alpha = 105.8°$, $\beta = 113.7°$, and $\gamma = 87.4°$. The triclinic structure was also reported for several semicrystalline polymers, such as polyethylene oxide, polyamide 66, and poly(ethylene terephthalate) [16]. By dividing the area under the crystalline reflections to the overall area of the XRD pattern, we obtained the bulk degree of crystallinity of PBOX of 0.23, 0.24, 0.24, and 0.27 crystallized at 70 °C, 75 °C, 80 °C, and 85 °C, respectively. It has to be pointed out that the measured intensities of the crystalline reflections may be smaller than the true value due to both the possible defects in the crystal lattice and the thermal disordering at high temperatures [17].

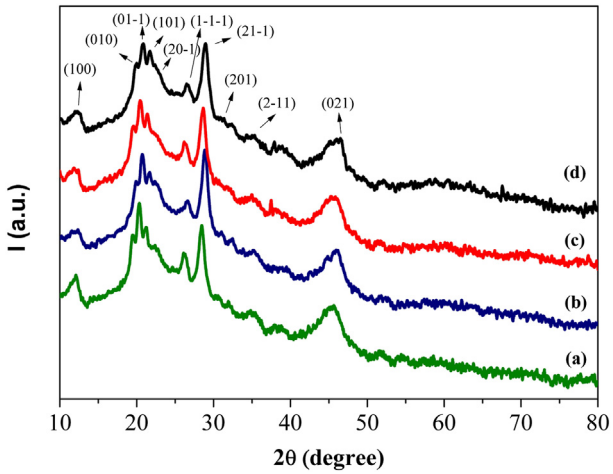

Fig. 1. XRD of PBOX crystallized at (a) 70 °C; (b) 75 °C; (c) 80 °C; and (d) 85 °C.

3.2. Crystalline morphology

Plots of the smoothed and extrapolated intensity profiles of the PBOX crystallized isothermally at selected temperatures are shown in Fig. 2. Fig. 3 shows the Lorentz-corrected intensities obtained in each experiment. For the PBOX, there was a significant induction time before any crystallization occurred. This was consistent with the observation that the melt-quenching procedure was sufficient to eliminate the crystals. During this period, the SAXS patterns show almost no crystal reflection peaks, and the morphological parameters cannot be calculated from the correlation function with good confidence. The induction time appears to be longer at higher crystallization temperature, which is attributed to the slow nucleation for small degree of supercooling. The longer induction time for PBOX crystallization prevents the polymer from crystallizing from the melt during sample preparation. After the induction period of crystallization, there was a gradual increase in the intensity of the low-angle scattering. In the later stage, the SAXS peak became well-developed and the diffraction peak indicated the stack of crystalline molecules. The lack of the higher order reflections of the primary peak is primarily because of polydispersity in the lamellar stack thickness [18–20].

Fig. 4 shows $\gamma(r)$ at various crystallization temperatures. Fig. 5 summaries 5 results of the morphological parameters (L, l_c, and l_a) of PBOX during crystallization. As previously mentioned, there are two possible solutions for W_c and it is not possible to mathematically distinguish between them. Our rational for using the smaller solution for W_c to calculate l_c was based on the low bulk degree of crystallinity obtained from XRD.

For PBOX crystallized at 70 °C, the long period decreased initially (for approximately the first 70 s). In the experiments for which the crystallization was allowed to continue beyond this time the long period only slightly decreased and slowly approached to a constant value. This decrease in the long period is attributed to the secondary crystallization in the interlamellar space [18]. On the contrary, the long periods for PBOX crystallized at higher temperatures showed a gradual increase during initial crystallization and reached a plateau. This behavior is presumably due to the slower nucleation at high temperatures, which reduced the occurrence of the secondary crystallization of PBOX. This is consistent with the Gibbs–Thomson theory on the crystallization behavior [21]. Fig. 6 summaries the long period, lamellar thickness, and amorphous thickness of PBOX after isothermal crystallization at long times. Both the long period and lamellar thickness slightly increased with crystallization temperature, meaning that thicker crystalline layers formed at high temperatures. This behavior is similar to the findings in several semicrystalline polymers, including poly(butylene terephthalate) [18], poly(ethylene terephthalate) [22], and isotactic polypropylene [23]. The increase in the lamellar thickness at higher temperature can be rationalized by the thermodynamics factors driven by the higher chain mobility and the greater ability of polymer segments to be disentanglement.

The temporal evolution of the linear degree of crystallinity for each experiment is shown in Fig. 7. For PBOX, the linear degree of crystallinity equilibrated within about 300 s at temperatures below 80 °C. At low temperatures, apparently the crystals formed very rapidly and only the brief period is required to heat the sample to the equilibrium. It is noted that the crystallinity obtained by SAXS and XRD techniques show consistency and W_c is slightly larger than the bulk degree of crystallinity (ϕ_c) determined by XRD. For the PBOX, the degree of crystallinity is too low to confidently assume

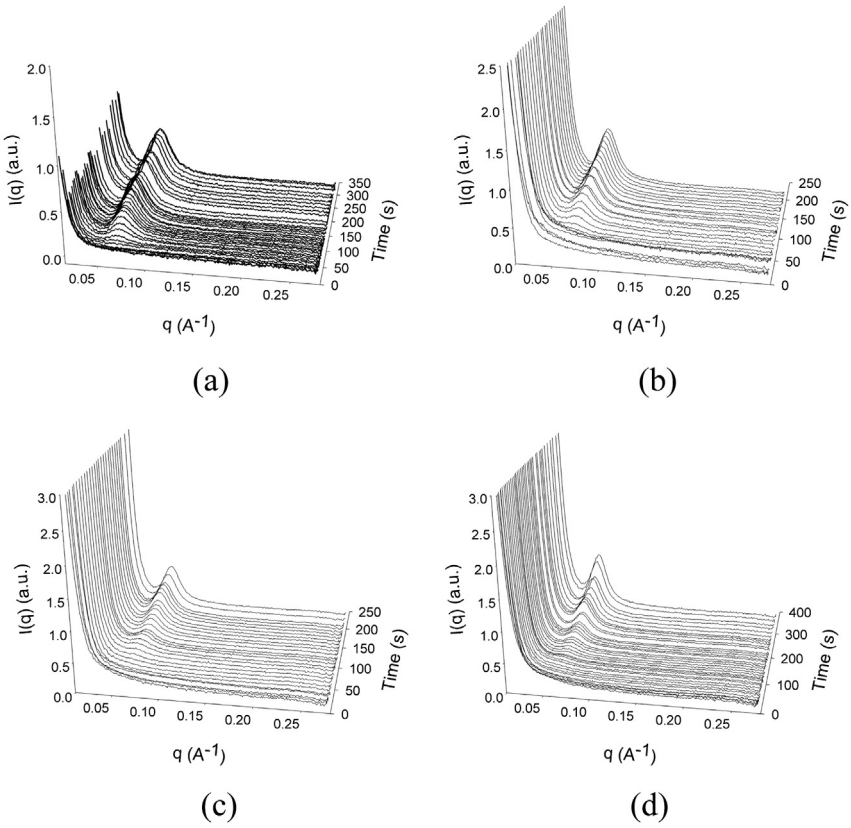

Fig. 2. The evolution of the SAXS patterns during isothermal crystallization at different temperatures. (a) 70 °C; (b) 75 °C; (c) 80 °C; and (d) 85 °C.

that the amorphous component is located only within the lamellar stacks. From our optical microscopy analysis, we obtain that there is no significant amount of material in interspherulitic regions as all spherulites impinge upon the completion of primary crystallization. Thus, we can conclude that the fraction of the amorphous material located in interfibrillar regions. This finding is consistent with the previous report that when $W_c > \phi_c$, a certain amount of the amorphous component resides in interfibrillar regions. On the other hand, $W_c = \phi_c$ indicates all of the amorphous component locating in interlamellar regions [24].

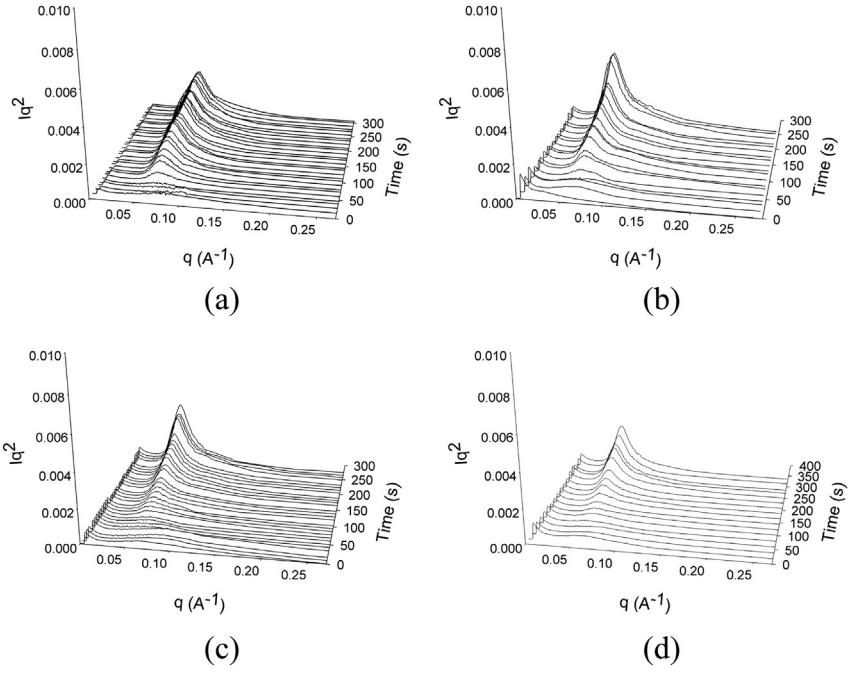

Fig. 3. Lorentz-corrected intensity profiles of PBOX isothermally crystallized at (a) 70 °C; (b) 75 °C; (c) 80 °C; and (d) 85 °C.

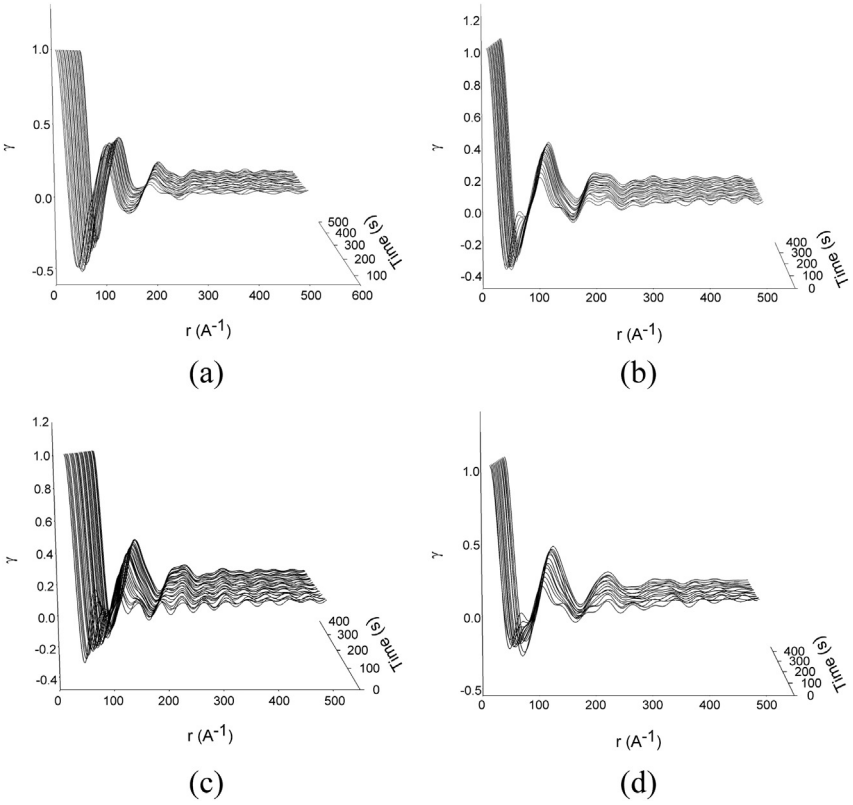

Fig. 4. $\gamma(r)$ profiles of PBOX crystallized at different temperatures. (a) 70 °C; (b) 75 °C; (c) 80 °C; and (d) 85 °C.

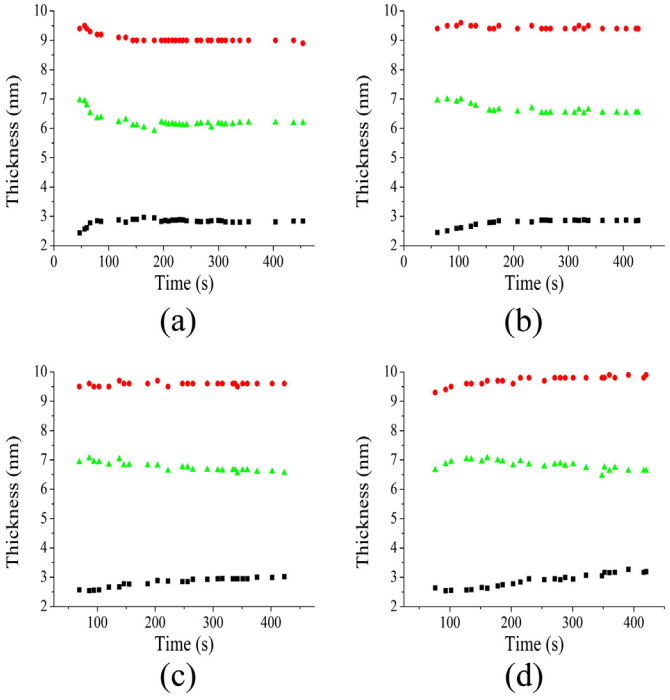

Fig. 5. The morphological parameters of PBOX obtained from SAXS as a function of crystallization temperature. (a) 70 °C; (b) 75 °C; (c) 80 °C; and (d) 85 °C. (●) L, (▲) l_a, and (■) l_c.

3.3. Equilibrium melting temperatures

The well-known approach for determining equilibrium melting temperatures of polymers is the Hoffman-Weeks method [21,25]. The Hoffman-Weeks method involves the extrapolation of a linear regression of experimentally observed melting temperatures (T_m) for various crystallization temperatures (T_c) to the equilibrium line $T_m = T_c$. This equation relates the initial stem length to the degree of supercooling and is based on the assumption that the difference between crystallization and the melting temperature is solely due to the thickening of lamellae formed at the crystallization temperature. Although data implementation using the Hoffman-Weeks method is straightforward, it has been demonstrated that this approach fails as a result of enhanced lamellar thickening for samples crystallized at the small degree of supercooling [25,26].

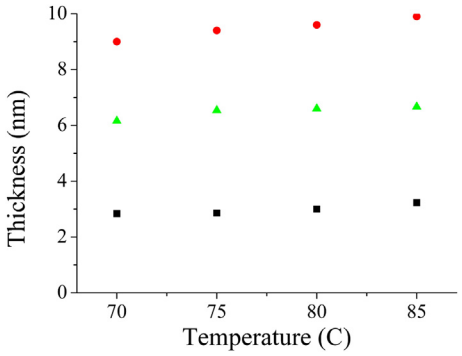

Fig. 6. The long period, lamellar thickness, and amorphous thickness of PBOX isothermally crystallized at long times. (●) L, (▲) l_a, and (■) l_c.

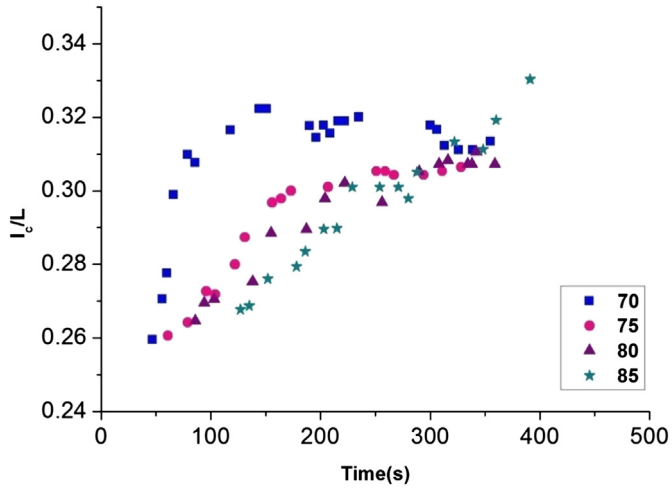

Fig. 7. Crystallinity parameters of PBOX crystallized at (a) 70 °C; (b) 75 °C; (c) 80 °C; and (d) 85 °C.

Meanwhile, the observation of a linear relationship between T_m and T_c is an indication that the lamellar thickening coefficient is constant. This is not always true because the lamellar thickening coefficient was reported to be dependent on polymer under consideration, the molecular weight of polymer, and the existence or absence of a crystalline α-relaxation of the crystalline polymer [27].

In comparison of the Hoffman-Weeks method, the Gibbs–Thomson approach is directly derived from thermodynamic relations, considering the excess free energy by the end surfaces [21]. The equation is given by

$$T_m = T_m^o\left(1 - \frac{2\sigma_e}{l_c \Delta H_f}\right) \tag{6}$$

Here, T_m^o is the equilibrium melting temperature, σ_e is the fold surface free energy, and ΔH_f is the heat of fusion of a perfect crystal. Because this approach is based solely on the thermodynamic arguments, it is correct and more reliable.

Fig. 8 shows the DSC heating diagrams of the PBOX crystals after a complete crystallization. The melting temperatures obtained

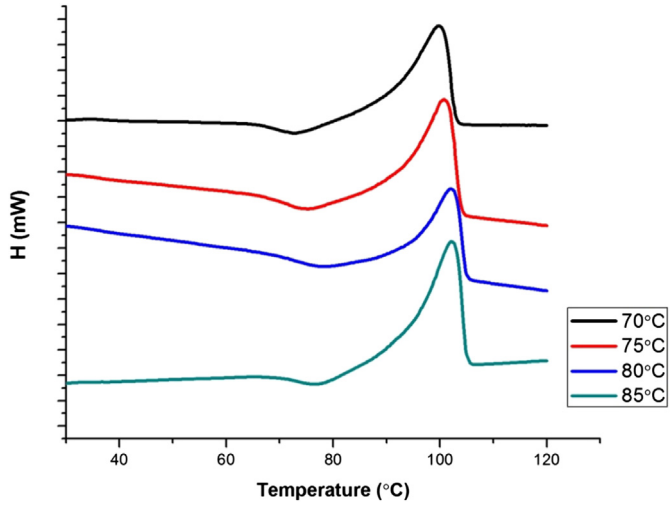

Fig. 8. DSC thermographs of PBOX annealed at different crystallization temperatures.

from DSC are 99.8 °C, 100.8 °C, 102.1 °C, and 102.2 °C for the crystallization temperature of 70 °C, 75 °C, 80 °C, and 85 °C, respectively. By taking ΔH_f^∞ as 158 J/g [9], the equilibrium melting temperature of PBOX extracted from the plot of T_m vs. $1/l_c$ is 117.4 °C and the fold surface free energy extracted from the slope of the linear extrapolation is 32.37 erg/cm^2. The literature value of the equilibrium melting temperature of PBOX is 100 °C, which was obtained using Baur's equation [9]. Since the equilibrium melting temperatures in two studies were obtained using different approaches, the difference between the above values may arise from model assumption. However, the same literature also reported the melting point of melt-quenched PBOX of 99 °C that is fairly close to their obtained T_m^o. It is unrealistic to believe that the melt-quenched sample can reach the ideal crystal with infinite crystal size. Therefore, it seems that the authors underestimate T_m^o and a larger value of T_m^o is much more realistic.

3.4. Spherulite growth rate

The morphology of PBOX was examined for samples crystallized in the temperature range from 70 to 85 °C by using optical microscopy. Few exemplary optical micrographs of PBOX, isothermally crystallized at 70 °C from the melt, are shown in Fig. 9. The crystal structure of the spherulites exhibited the typical Maltese cross pattern under the polarizing microscope, which was caused by the different light refractivity between crystalline and amorphous phases. Those spherulites grew starting from nucleation sites and followed by the growth of spherulites. In the later stage, the spherulites impinged with neighbors, forming polycrystalline structure. Radial growth ceased only when all surfaces were bounded. In Fig. 10, the spherulite radii (R_a) are plotted against time for PBOX crystallized at various constant temperatures. It is noted that only the rates measured before the impingement of the spherulites are used in the plot. These data clearly show that the radius of the spherulites grew linearly with time. The nearly linear relationship suggests that the growth rates were independent of the size of the spherulites. The slope of the curves, dR_a/dt, systematically decreased as the melting point was approached. At high temperatures, the degree of supercooling is small. As a result, the nucleation rate reduced, causing the decreasing overall crystal growth rate. According to the calculated spherulite growth rates ($G = dR_a/dt$), PBOX exhibited relatively slow crystal growth rates (0.02 μm/s at 85 °C and 0.12 μm/s at 70 °C), which are much smaller than that of polyethylene (G = 83.3 μm/s) [28], but are comparable to various semicrystalline polymers, including polypropylene (G = 0.3 μm/s) [29], poly(ethylene terephthalate) (G = 0.17 μm/s) [30], and isotactic polystyrene (G = 0.033 μm/s) [31].

The growth rate of polymers during crystallization was described in a given regime by Lauritzen and Hoffman [32]

$$G = G_0 \exp\left(\frac{-U^*}{R(T_c - T_\infty)}\right)\exp\left(-\frac{K_g}{T_c \Delta T f}\right) \tag{7}$$

here, G_0 is the pre-exponential factor, $\Delta T = T_m^o - T_c$ is the degree of supercooling, $f = 2T_c/(T_m^o + T_c)$ is the correction factor, and R is the gas constant. K_g is the nucleation constant in which n is 4 for regimes I and III and 2 for regime II.

$$K_g = \frac{n b_0 \sigma \sigma_e T_m^o}{\Delta H_f k_B} \tag{8}$$

here, σ is the lateral surface free energy and k_B is the Boltzmann constant.

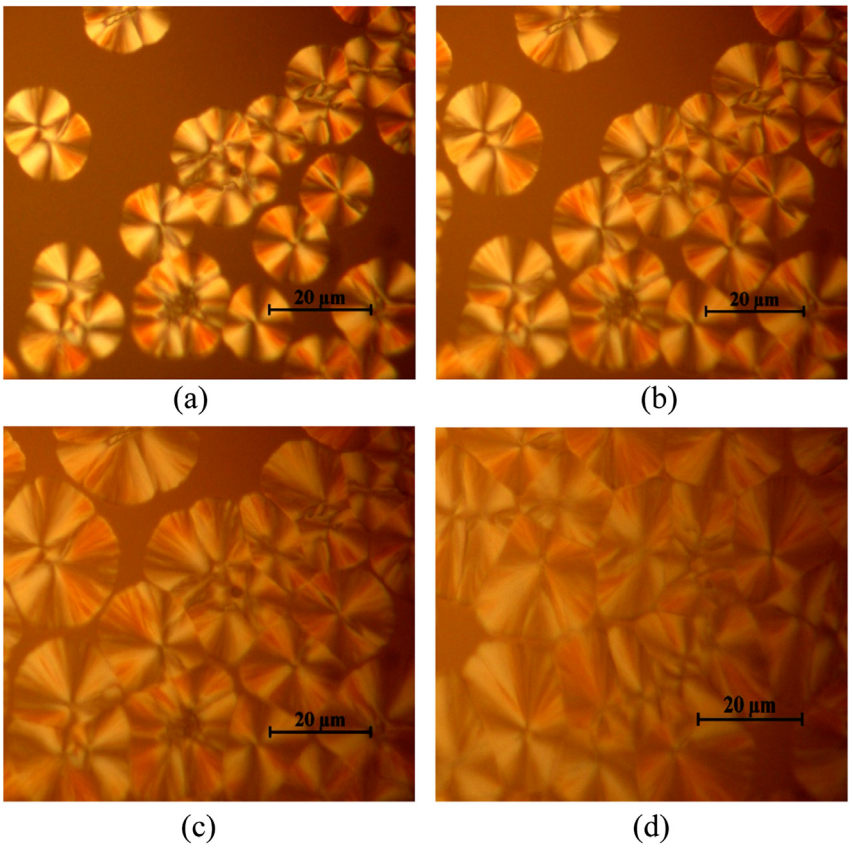

Fig. 9. Spherulite growth of PBOX at 70 °C with time. (a) 36 s; (b) 50 s; (c) 84 s; and (d) 124 s.

The first exponential term in Eq. (7), $\exp(-U^*/R(T_c - T_\infty))$, indicates the chain transport effect on the interface. The second term, $\exp(-K_g/T_c\Delta Tf)$, represents the secondary nucleation effect. The nucleation constants, K_g and G_0, can be obtained by a plot from the Eq. (7) in the form of $[\ln(G) + U^*/R(T_c - T_\infty)]$ vs. $[1/(T_c\Delta Tf)]$. The widely used values for U^* and T_∞ are 1500 cal/mol and T_g−30 K, where T_g is the glass transition temperature, for a large number of polymers [25,33]. By the growth rates determined earlier from the slopes of the lines displayed in Fig. 10, the result of the Lauritzen and Hoffman analysis for PBOX crystallization is shown in Fig. 11. A good linear relationship was reached, yielding a value of 97264 K^2 for K_g.

Because the determination of the surface free energy product ($\sigma\sigma_e$) in Eq. (8) is complicated by an uncertainty of the crystallization regime, we utilized the Lauritzen *Z*-test in Eq. (9) to distinguish between regimes I and II, but regime III is not considered in this approach [32].

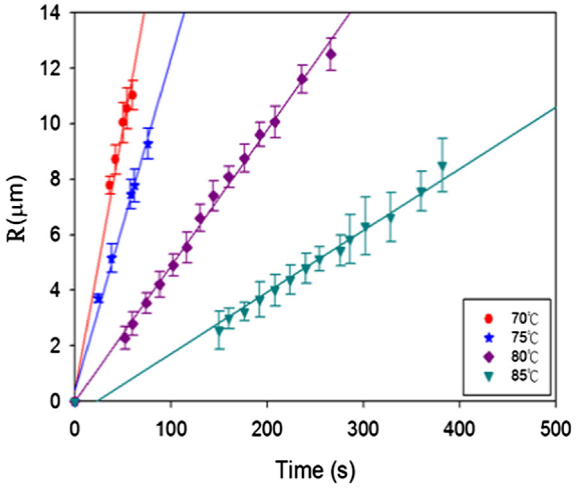

Fig. 10. The radius of the spherulites of PBOX as a function of time and temperature.

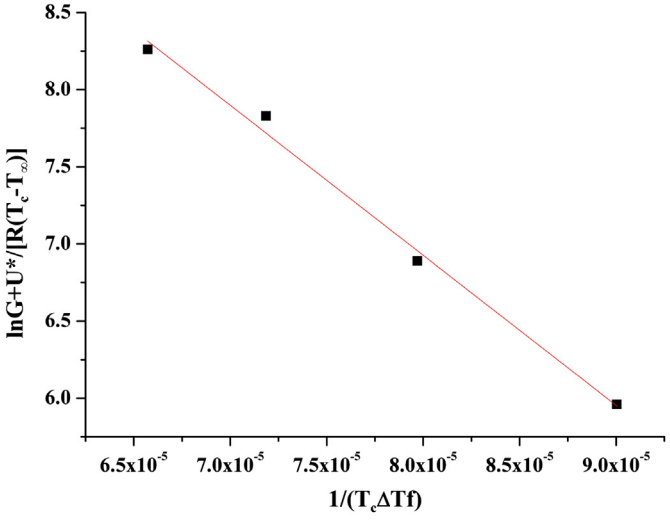

Fig. 11. The Plot of $[\ln G + U^*/R(T_c - T_\infty)]$ vs. $[1/T_c\Delta Tf]$ for PBOX.

Table 1
Comparison of the growth rate parameters for several polymers.

Polymer	σ (erg/cm^2)	σ_e (erg/cm^2)	$\sigma\sigma_e$ (erg^2/cm^4)	$K_g \times 10^{-5}$ (K^2)	Reference
PBOX	17.68	32.37	572.3	0.97	This work
Poly(trimethylene terephthalate)	10.89	56.64	616.8	1.45	[35]
Poly(butylene terephthalate)	8.8	57	501.6	0.53	[35]
Poly(ethylene terephthalate)	10.6	140	1484	2.81	[35]
Poly-L-lactic acid	15.3	53	813	2.44	[36]
Polyethylene	11.8	90	1063	0.96	[36]
Nylon-11	10.65	110.62	1181.42	1.66	[37]
Poly(aryl ether ether ketone)	38.0	41–101	1587–3656	8.0–18.2	[38]

$$Z \approx 10^3 \left(\frac{L_0}{2a_0}\right)^2 \exp[(-X/(T_c\Delta T))] \quad (9)$$

where L_0 is the effective lamellae width. If $X = K_g$ yields $Z \leq 0.01$, crystallization follows regime I. On the contrary, if $X = 2\ K_g$ leads to $Z \geq 1$, the regime II kinetics is obeyed. As pointed out by Hoffman and Lauritzen [32] and Wang and Nishi [34], it is more convenient to use the known values of K_g and the inequalities for the Z value to obtain the value of L_0 in the two regimes and then further to justify the realistic of such values. Application of the Z test to the PBOX in the entire range of T_c leads to the following results. If crystallization occurs in regime I, L_0 cannot be more than 0.107 nm. This is clearly unrealistic. In contrast, if the crystallization is assumed to be in regime II, L_0 is greater than 0.049 nm. Based on this simple calculation, the crystallization of PBOX follows the regime II and the value of n was substituted by 2 in Eq. (8).

According to the regime II crystallization and the obtained value of K_g, the lateral surface free energy is calculated to be 17.68 erg/cm^2. A condensed list of the important growth rate parameters obtained from several polymers that are available in the literature is given in Table 1. The discrepancy between those studies could potentially be attributed to the contributions from differences in the chain-folding regularities of the various polymers. In addition, since these polymers have different molecular weights, they exhibit different numbers of intercrystalline links and chain entanglements. Those, in turn, can affect molecular motion in the polymer melt and so increase in the degree of disorder in the intercrystalline region of the crystallized polymers. Although it is unable to justify and compare our obtained parameters from the reported data, it is fair to conclude that the obtained growth rate parameters for PBOX are in the reasonable range.

4. Conclusion

Morphological changes of PBOX during isothermal crystallization were observed via *in situ* SAXS. The correlation function approach was used to extract trends in the morphological details at the lamellar level. The SAXS results indicate that the decrease in the long period at low temperature was related to the formation of secondary crystal lamellae between the primary lamellar stacks during isothermal crystallization. In contrast, the long periods for PBOX crystallized at higher temperatures showed a gradual increase during initial crystallization and reached a plateau. This behavior is associated to the slower nucleation at high temperatures, which reduced the occurrence of the secondary crystallization of PBOX. The crystal growth rates of PBOX crystallized at desired temperatures were determined by polarized optical microscopy. Results reveal that PBOX crystallized in a spherulitic form and the spherulite growth rate deceased with an increase in the crystallization temperature due to the low degree of supercooling. Additionally, PBOX follows regime II crystallization. Using the determined equilibrium melting temperature and the fold surface free energy, the nucleation parameter, K_g, of 97264 K^2 and the lateral surface free energy of 17.68 erg/cm^2 were obtained from the Lauritzen and Hoffman equation. This work also provides a quantitative structural description of the lamellar thickness and degree of crystallinity. These microstructural characterizations are an essential element of many applications.

Acknowledgments

This work is financially supported by National Science Council in Taiwan under Grant No. NSC 99-2628-E-006-001 and the Technology Development Program for Academia No. 101-EC-17-A-08-S1-204 by Ministry of Economic Affairs in Taiwan.

References

[1] Carothers WH, Dorough GL, Van Natta FJ. J Am Chem Soc 1932;54:761–72.
[2] Holland SJ, Tighe BJ, Gould PL. J Control Release 1986;4:155–80.
[3] Kim S, Seong K, Kim O, Kim S, Seo H, Lee M, et al. Biomacromolecules 2010;11:555–60.
[4] Lee E, Kim S, Seong K, Park H, Seo H, Khang G, et al. J Biomater Sci Polym Ed 2011;22:1683–94.
[5] Abu-Awwad IF, Khalili FI, Sweileh BA. Solvent Extr Ion Exch 2010;28:682–705.
[6] Ballistreri A, Garozzo D, Giuffrida M, Impallomeni G, Montaudo G. Polym Degrad Stab 1988;21:311–21.
[7] Thibeault B, Stickles EM, Weininger SJ, Remy DE. J Polym Sci Polym Chem Ed 1990;28:1361–76.
[8] Alksnis A, Deme D. J Polym Sci Polym Chem Ed 1979;17:2701–6.
[9] Finelli L, Lotti N, Munari A. Eur Polym J 2002;38:1987–93.
[10] Kipper MJ, Seifert S, Thiyagarajan P, Narasimhan B. J Polym Sci Polym Phys Ed 2005;43:463–77.
[11] Andjelic S, Jamiolkowski DD, Bezwada R. Polym Int 2007;56:1063–77.
[12] Verma RK, Velikov V, Kander RG, Marand H, Chu B, Hsiao BS. Polymer 1996;37:5357–65.
[13] Debye P, Bueche AM. J Appl Crystallogr 1949;20:518–25.
[14] Ruland W. J Appl Crystallogr 1971;4:70–3.
[15] Strobl GR, Schneider M. J Polym Sci Polym Phys Ed 1980;18:1343–59.
[16] Tadokoro H. Structure of crystalline polymers. New York: Wiley-Interscience; 1979.
[17] Wang ZG, Wang XH, Hsiao BS, Phillips RA, Medellin-Rodriguez FJ, Srinivas S, et al. J Polym Sci Polym Phys Ed 2001;39:2982–95.
[18] Hsiao BS, Wang ZG, Yeh F, Gao Y, Sheth KC. Polymer 1999;40:3515–23.
[19] Wang ZG, Hsiao BS, Fu BX, Liu L, Yeh F, Sauer BB, et al. Polymer 2000;41:1791–7.
[20] Hama H, Tashiro K. Polymer 2003;4:2159–68.
[21] Hoffman JD, Davis GT, Lauritzen JI. The rate of crystallization of linear polymers with chain folding. In: Hannay NB, editor. Treatise on solid state chemistry, vol. 3. New York: Plenum; 1976. p. 497–614.
[22] Wang ZG, Hsiao BS, Sauer BB, Kampert WG. Polymer 1999;40:4615–27.
[23] Wang ZG, Hsiao BS, Sirota EB, Agarwal P, Srinivas S. Macromolecules 2000;33:978–89.
[24] Huang J, Lisowski MS, Runt J, Hall ES, Kean RT, Buehler N, et al. Macromolecules 1998;31:2593–9.
[25] Hoffman JD, Miller RL. Polymer 1997;38:3151–212.
[26] Alamo RG, Viers BD, Mandelkern L. Macromolecules 1995;28:3205–13.
[27] Marand H, Xu J, Srinivas S. Macromolecules 1998;31:8219–29.
[28] Price FP. J Phys Chem 1960;64:169–70.
[29] Falkai VBV. Die Makromolekulare Chem 1960;41:86–109.
[30] Keller A, Lester GR, Morgan LB. Phil Trans R Soc Lond A 1954;247:1–12.
[31] Boon J, Challa G, Vankreve DW. J Polym Sci Polym Phys Ed 1968;6:1791.

[32] Lauritzen JI, Hoffman JD. J Appl Phys 1973;44:4340–52.
[33] Hoffman JD. SPE Trans 1964:315–62.
[34] Wang TT, Nishi T. Macromolecules 1977;10:421–5.
[35] Huang JM, Chang FC. J Polym Sci Polym Phys Ed 2000;38:934–41.
[36] Hoffman JD, Miller RL, Marand H, Boltman DB. Macromolecules 1992;25:2221–9.
[37] Liu S, Yu Y, Chi Y, Zhang H, Mo Z. J Appl Polym Sci 1998;70:2371–80.
[38] Deslandes Y, Sabir FN, Roovers J. Polymer 1991;32:1267–73.